Applied Catalysis B: Environmental 125 (2012) 367–374

Contents lists available at SciVerse ScienceDirect

Applied Catalysis B: Environmental

journal homepage: www.elsevier.com/locate/apcatb

Hierarchical $SrTiO_3/TiO_2$ nanofibers heterostructures with high efficiency in photocatalytic H_2 generation

Hongwei Bai, Jermyn Juay, Zhaoyang Liu*, Xiaoxiao Song, Siew Siang Lee, Darren Delai Sun*

School of Civil & Environmental Engineering, Nanyang Technological University, Singapore 639798, Singapore

ARTICLE INFO

Article history:
Received 20 April 2012
Received in revised form 6 June 2012
Accepted 12 June 2012
Available online 21 June 2012

Keywords:
Heterostructure
Hierarchical
H_2 Generation
$SrTiO_3$
TiO_2

ABSTRACT

Through hydrothermally growing $SrTiO_3$ cubics on the surface of electrospun TiO_2 nanofibers, $SrTiO_3/TiO_2$ nanofibers heterostructures were successfully fabricated in the present study. This process is able to ensure uniform distribution of $SrTiO_3$ on the surface of TiO_2 nanofibers and lead to close contact between $SrTiO_3$ and TiO_2, which is beneficial for the fast separation of photogenerated electrons and holes so as to suppress the recombination of photogenerated electrons and holes at the interphase of $SrTiO_3$ and TiO_2. Besides this, the long 1D fibrous structure easy for electron transfer, the hierarchical structure promoting mass transfer and allowing more light reflection and absorption, and the large specific surface area providing more reactions sites to facilitate the reactants to desired oxidation places all together create a synergistic effect on improving the photocatalytic activity of the hierarchical $SrTiO_3/TiO_2$ nanofibers heterostructures. Under the irradiation of UV light, in a water/methanol sacrificial reagent system, the $SrTiO_3/TiO_2$ nanofibers heterostructures generate five times more H_2 than bare TiO_2 nanofibers because of its high photocatalytic activity.

1. Introduction

The threats rising from the overdependence on the fast depleted fossil fuels and the global challenge of increasingly severe climate change make it pressing to seek for an alternative energy to create a green world for our future generations [1–4]. Hydrogen (H_2) energy proved to be a promising clean energy source owing to its intrinsic properties such as pollutant-free and high energy intensity, and thus attracting huge amount of research efforts throughout the world [5]. The discovery of photoelectrochemical splitting water by an UV irradiated TiO_2 photoelectrode in 1972 inspires us to make full use of sun light to photocatalytically generate H_2 [6]. Since semiconductor photocatalyst plays a key role in the photocatalytic H_2 generation process, much more attention has been focused on TiO_2 water splitting with various TiO_2 nanomaterials being developed [7–9].

The performance of TiO_2 was significantly related to its crystalline phase, morphology and dimensionality [10–12]. High crystallinity and specific surface area is reported to be positively affect the surface-based photocatalytic reaction such as heterogeneous photocatalysis in achieving high photocatalytic activity depending on their induced shape- and size-properties [13]. In the past decades, considerable attentions have been paid to one dimensional (1D) TiO_2 nanomaterials such as wires, tubes, rods and belts, due to their significant roles in providing large interfacial areas and channels favorable for effective separation of photogenerated electrons and holes, thus suppressing their recombination to enhance the photocatalytic activity [14]. A variety of 1D TiO_2 nanomaterials have been widely applied in photocatalysis, photoelectrochemical process, and dye sensitized solar cells, etc [15–18]. Particularly, numerous research efforts have been devoted to developing TiO_2 nanofibers. Electrospinning is a remarkable versatile and fantastic technique for the fabrication of continuous TiO_2 nanofibers with diameters down to few nanometers [19–21]. As a photocatalyst, the electrospun TiO_2 nanofibers exhibit excellent advantages such as high specific surface areas to facilitate the access of reactants, porous and rough surface easy for light reflection and absorption, three-dimensional open structure, and favorable fibrous morphology boosting electrons delocalization, those virtues create a synergistic effect on the improvement of photocatalytic activity [14,22]. However, the broad application of TiO_2 nanofibers in photocatalytic pollutants removal and H_2 generation is still greatly limited by its comparatively low photocatalytic activity due to its wide band gap and fast recombination of photogenerated electrons and holes [23]. It is a good approach to improve the photocatalytic activity of TiO_2 nanofibers via coupling with other semiconductor such as V_2O_5/TiO_2 [24], TiO_2/SnO_2 [23], TiO_2/ZnO [25], etc. In the coupled structure, the interphase formed between semiconductors with different bandgaps is beneficial for the

* Corresponding authors.
E-mail addresses: zyliu@ntu.edu.sg (Z. Liu), ddsun@ntu.edu.sg (D.D. Sun).

0926-3373/$ – see front matter © 2012 Elsevier B.V. All rights reserved.
http://dx.doi.org/10.1016/j.apcatb.2012.06.007

electron transfer and separation so as to improve the photocatalytic activity via suppressing their recombination [25,26].

$SrTiO_3$, as a well-known cubic-perovskite-type multimetallic oxide with a band gap of 3.7 eV has attracted considerable attentions because of its wide applications in photocatalysis, and photoelectrodes for dye-sensitized solar cells [27,28]. The conduction band (CB) edge of $SrTiO_3$ is 200 mV more negative than TiO_2, therefore the proper couple of $SrTiO_3$ and TiO_2 would lead to not only the transfer of electron from the CB of $SrTiO_3$ to that of TiO_2, but also the transfer of holes from the valence band (VB) of TiO_2 to that of $SrTiO_3$ [26]. In such an approach, an improved separation of photogenerated electrons and holes is achieved in the coupled $SrTiO_3/TiO_2$ heterostructure, so as to benefit the photocatalytic activity improvement [26]. And the closer the contact between $SrTiO_3$ and TiO_2 is, the more the increase in photocatalytic activity of hetero-$SrTiO_3/TiO_2$ will be [29,30]. Wherefore, the close contact between $SrTiO_3$ and TiO_2 is of significant importance to promote the separation of photogenerated electrons and holes [22].

Taking the abovementioned considerations into account, we have successfully fabricated $SrTiO_3/TiO_2$ nanofibers heterostructures in the present study. The $SrTiO_3$ cubics were uniformly growing on the surface of electrospun TiO_2 nanofibers forming hierarchical $SrTiO_3/TiO_2$ nanofibers heterostructures. The hydrothermal growing process occurred on the surface of TiO_2 nanofibers is able to ensure the close contact between $SrTiO_3$ and TiO_2. Such a close contact between $SrTiO_3$ and TiO_2 as well as the favorable fibrous structure would synergistically promote the effective separation of photogenerated electrons and holes and thus improving the photocatalytic activity, which is proved by its higher photocatalytic H_2 generation activity in a comparison to bare TiO_2 nanofibers.

2. Experimental

2.1. Chemicals

Polyvinylpyrrolidone (PVP, Mn 1,300,000) was purchased from Sigma–Aldrich), while titanium butyloxide ($Ti(OBu)_4$), $Sr(NO_3)$ power, and NH_4OH solution were purchased from Merck & Co., Inc. Absolute ethanol (>99.9%, Fisher) and deionized (DI) water (Millipore) with a resistance greater than 18 MΩ were used as the solvent for the materials synthesis. The TiO_2 nanofibers were prepared by electrospinning, and $SrTiO_3/TiO_2$ nanofibers heterostructures were fabricated by hydrothermally growing $SrTiO_3$ nanocubics on the surface of as-spun TiO_2 nanofibers.

2.2. Fabrication of TiO_2 nanofibers by electrospinning

Under continuous stirring, dissolve 0.6 g polyvinylpyrrolidone (PVP Mn 1,300,000) into 10 mL of absolute ethanol, then 2.3 mL $(Ti(OBu)_4$ was added in the mixed solution. The well prepared precursor solution was continuously stirred for 8 h to form a clear and homogeneous solution ready for electrospinning TiO_2 nanofibers [23,24]. Here, a self-designed setup was used for electrospinning TiO_2 nanofibers as our previously reported [23–25]. Humidity greatly affects the morphology evolution of electrospun TiO_2 nanofibers, therefore the humidity inside the electrospinning chamber was maintained at <40% by continuously purging N_2 gas throughout the electrospinning process to prevent pre-mature hydrolysis of the precursor solution [31,32]. A plastic capillary with an inner diameter of 0.5 mm was used as the spinneret with a spinning speed of 5–10 μL/min. A DC high voltage power supply was employed to provide an applied voltage of 20 kV, a non-woven mat of PVP/$Ti(OBu)_4$ composite was collected on a grounded aluminum foil at an electrode distance of 18 cm. After exposure to air for complete hydrolysis, the as-spun non-woven mats were calcined at 550 °C in air for 1 h, with a temperature rise step at 2 °C/min.

2.3. Fabrication of $SrTiO_3/TiO_2$ nanofibers heterostructures

A typical procedure was developed to prepare the precursor solution for hydrothermally growing $SrTiO_3$ cubics on the surface of as-spun TiO_2 nanofibers to fabricate the $SrTiO_3/TiO_2$ nanofibers heterostructures. Firstly, 2.5 g $Sr(NO_3)_2$ powder was dissolved in the mixed solution of 40 mL DI water and 40 mL NH_4OH. Then 100 mg as-spun TiO_2 nanofibers were well dispersed in the solution, the well prepared precursor solution was transferred to a 125 mL Teflon-lined autoclave. The autoclave was heated in an electron oven for 48 h at 180 °C [22,26,33]. After cooling down naturally, the collected white precipitates from the autoclave was thoroughly washed with DI water before further characterization and activity evaluations. As a reference, $SrTiO_3$ nanocubics were also prepared using the same hydrothermal method as above but without the addition of TiO_2 nanofibers.

2.4. Characterizations

The morphology of the bare TiO_2 nanofibers and $SrTiO_3/TiO_2$ nanofibers heterostructures were observed by field emission scanning electron microscopy (Jeol, JSM 7600F) and transmission electron microscopy (TEM) (Jeol, JSM2010). An energy dispersive X-ray spectrometer (EDS) detector (Oxford, 80 mm^2) attached to the FESEM was used to measure the element composition and distribution. A scanning transmission electron microscopy (STEM) detector attached to the FESEM was also used to take FESEM-STEM images of the samples. The structure and crystal phase of the bare TiO_2 nanofibers and $SrTiO_3/TiO_2$ nanofibers heterostructures were measured by X-ray diffractometer (Bruker AXS D8 Advance, GmhH, Karlsruhe, Germany) with monochromated high-intensity CuKα radiation (λ = 1.5418 Å) across a 2θ range of 10–80°, with a step size of 0.0050° and a step time of 2.0 s. The analysis was carried out at a voltage of 40 kV and an accelerating current of 30 mA. The obtained spectra were then matched with a Powder Diffraction File (PDF) database maintained by the International Centre for Diffraction Date (ICDD). The chemical composition and electron structure of the bare TiO_2 nanofibers and $SrTiO_3/TiO_2$ nanofibers heterostructures were measured by a Kratos Axis Ultra X-ray photoelectron spectrometer (XPS) with a monochromic AL Kα source at 1486.7 eV, with a voltage of 15 kV and an emission current of 10 mA. The carbonaceous C 1s line of 284.6 eV was used as the reference to calibrate the binding energies (eV). Ultraviolet–visible (UV–vis) diffuse reflection spectra of the bare TiO_2 nanofibers and $SrTiO_3/TiO_2$ nanofibers heterostructures were recorded by a Thermo Scientific Evolution 300 UV–vis spectrometer (Thermo Scientific, Massachusetts, USA) equipped with an integrating sphere assembly and a Xenon lamp source. The porous structure of the bare TiO_2 nanofibers and $SrTiO_3/TiO_2$ nanofibers heterostructures were characterized by a N_2 adsorption/desorption isotherm using a Micromeritics ASAP 2040 system at liquid nitrogen temperature (77 K). Before the measurement, 0.1 g sample was out-gassed under vacuum for 6 h at 250 °C. Pore volume and size distributions were derived from the desorption branches of the isotherms by the Barrett–Joyner–Halenda (BJH) model, and the Brunauer–Emmett–Teller (BET) equation was used to calculate the specific surface area from the adsorption data.

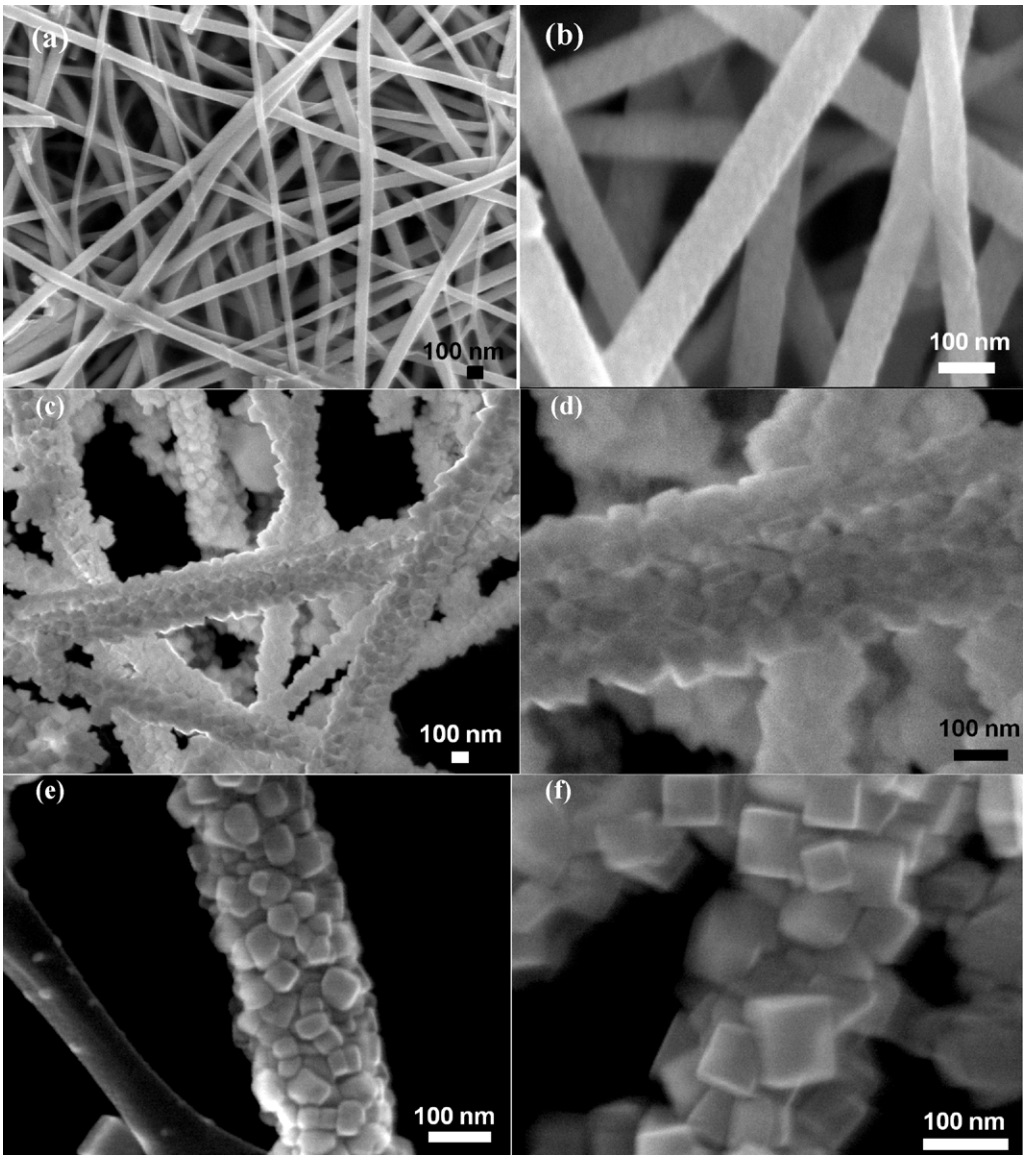

Fig. 1. FESEM images of (a)–(b) bare TiO_2 nanofibers, and (c)–(f) $SrTiO_3/TiO_2$ nanofibers heterostructures at different magnifications.

2.5. Evaluation of photocatalytic H_2 generation activity

The well prepared $SrTiO_3/TiO_2$ nanofibers heterostructures were investigated for photocatalytic H_2 generation in a methanol/water sacrificial reagent system under the irradiation of UV light. The photocatalytic H_2 generation test was carried out in an inner irradiation type Pyrex reactor with a volume of 270 mL with a 400 W high pressure Hg lamp (Riko, UVL-400HA) as the light source. The reactor was wrapped with a cooling water jacket with re-circulated tap water to maintain a constant reactor temperature of 298 K. The $SrTiO_3/TiO_2$ nanofibers heterostructures at a concentration of 0.5 g/L was suspended into the mixed methanol/water solution on a magnetic stirrer to form homogeneous reaction solution. Prior to irradiation, the reactor was purged thoroughly with nitrogen gas for 30 min to de-aerate the reactor. The H_2 gas generated from the photocatalytic reaction was collected by a water replacement trap and was analyzed using a TCD-type gas chromatography (Agilent 7890A, HP-PLOT MoleSieve/5A) [34,35]. As a reference, activities of bare TiO_2 nanofibers and bare $SrTiO_3$ nanocubics were also investigated under the same conditions.

3. Results and discussion

3.1. Materials characterizations

The morphologies of the as-spun bare TiO_2 nanofibers and the $SrTiO_3/TiO_2$ nanofibers heterostructures were observed by FESEM, with the images shown in Fig. 1. The bare TiO_2 nanofiber appears to be long fibrous structure with a length of tens of micrometers and a diameter of less than 100 nm. Such a long fibrous structure is favorable for fast electron transfer and is easy for handling and recycling [23]. The high temperature calcination in the furnace aims at burning off polymers bonding the Ti precursor, and promoting the crystallization of TiO_2. Hence, the porous rough surface of the TiO_2 nanofibers is clearly visible, which is resulted from the crystallized TiO_2 nano-knots [25]. Those porous positions on the rough surface of TiO_2 nanofibers are postulated to act as the nucleation roots for the $SrTiO_3$ cubics. Under the condition of high temperature and pressure in the autoclave, the $SrTiO_3$ cubics were uniformly growth on the surface of bare TiO_2 nanofibers forming $SrTiO_3/TiO_2$ nanofibers heterostructures, which is witnessed by the FESEM images in Fig. 1c and d. Furthermore, from the FESEM images

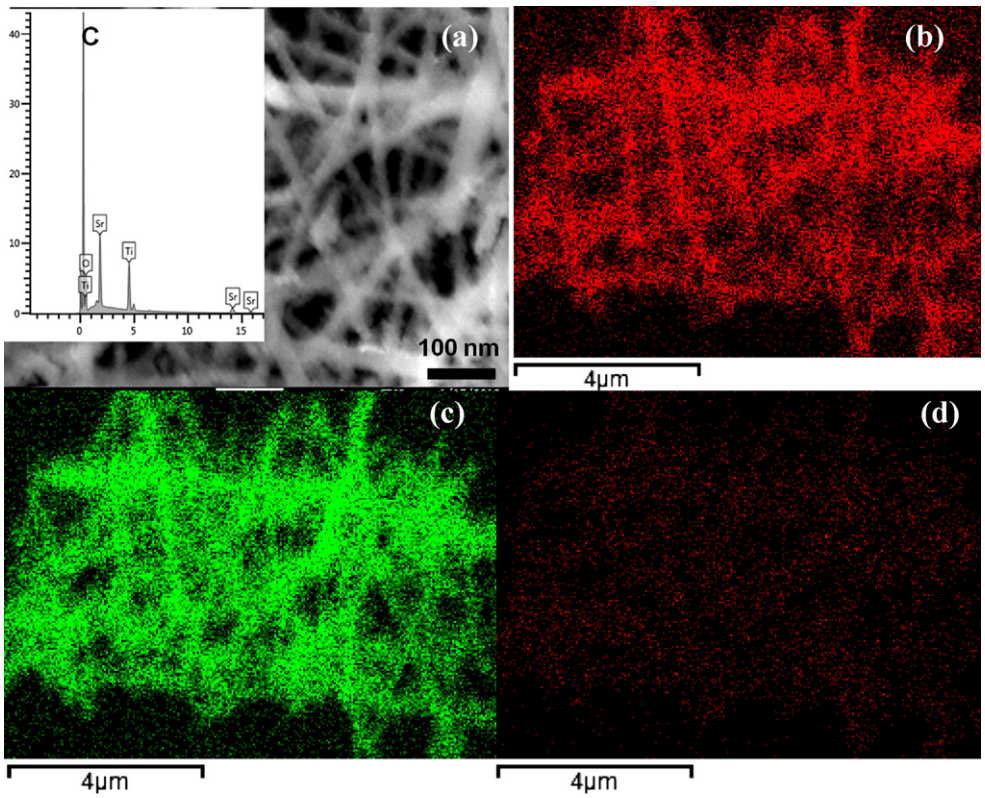

Fig. 2. (a) EDS spectrum, and element mapping of (b) O, (c) Ti and (d) Sr of the $SrTiO_3/TiO_2$ nanofibers heterostructures of the area in (a).

taken at high magnifications in Fig. 1e and f, the cubic structure of $SrTiO_3$ on the surface of TiO_2 nanofibers is closely contact to each other. The dimension of $SrTiO_3$ cubic is around tens of nanometers. The distance between $SrTiO_3$ cubic is around 10 nm, while the distance between different $SrTiO_3/TiO_2$ nanofibers heterostructures is in the range of micrometers, indicating its typical hierarchical structure property [25]. As being widely studied, the hierarchical structure possess the capability in enlarging specific surface area for mass transfer to ease the access of reactant, and allowing more light reflection and absorption inside the structure. Naturally, the hierarchical structure brings another virtue to benefit the improvement of photocatalytic activity [36,37].

An Oxford EDS detector attached to the FESEM is used to measure the element composition and distribution of the $SrTiO_3/TiO_2$ nanofibers heterostructures. From the EDS spectrum in the inset of Fig. 2a, it is clear to see that O, Sr, Ti dominates the composition of the $SrTiO_3/TiO_2$ nanofibers heterostructures, while the obvious external carbon is inevitable during the measurement [30]. The atomic ratio of Sr:Ti was revealed to be 1:1 in the $SrTiO_3/TiO_2$ nanofibers heterostructures by the EDS analysis. Fig. 2b–d are the elements mapping images of O, Ti and Sr of the $SrTiO_3/TiO_2$ nanofibers heterostructures shown in Fig. 2a, respectively. Those mapping images are solid proofs that the O, Sr and Ti are uniformly distributed in the $SrTiO_3/TiO_2$ nanofibers heterostructures. This further consolidates that $SrTiO_3$ and TiO_2 are close contact to each other, which is in favor of the separation of photogenerated electrons and holes to promote the photocatalytic activity improvement [26].

TEM analysis was carried out to further elucidate the crystal structure of the $SrTiO_3/TiO_2$ nanofibers heterostructures. The TEM images of bare TiO_2 nanofibers at low and high magnifications were shown in Fig. 3a and b, respectively. The rough surface of TiO_2 nanofibers is clearly visible and is in consistent with that observed by FESEM in Fig. 1b. After being hydrothermally treated in a the mixture of NH_4OH and $Sr(NO_3)_2$ solution in the autoclave, $SrTiO_3$ cubic was uniformly growth on the surface of TiO_2 nanofibers. The FESEM-STEM images of $SrTiO_3/TiO_2$ nanofibers heterostructures are shown in Fig. 3c and d at low and high magnifications, respectively. The dimension of the $SrTiO_3$ cubic is around tens of nanometers, which is in line with the observation of FESEM images in Fig. 1c and d. And the close contact between different $SrTiO_3$ cubics is revealed again. HRTEM image of the bare TiO_2 nanofibers is shown in Fig. 3e, the fringe lattice spacing of bare TiO_2 nanofibers is around 0.352 nm consonant to the energetically stable crystal faces of TiO_2 [1 0 1]. The selected area electron diffraction (SAED) pattern in the inset of Fig. 3e is a typical TiO_2 polycrystalline structure [26]. Fig. 3f displays an overlapping area of $SrTiO_3$ and TiO_2 in the $SrTiO_3/TiO_2$ nanofibers nanostructures. The respective interlayer distances were ascribed to the energetically stable crystal faces of TiO_2 [1 0 1] and $SrTiO_3$ [1 1 0] [26]. Obviously, the $SrTiO_3$ cubics were grown in conjunction with TiO_2 nanofibers forming a typical $SrTiO_3/TiO_2$ nanofibers heterostructures.

XRD analysis was conducted to reveal the crystal structures of bare TiO_2 nanofibers and $SrTiO_3/TiO_2$ nanofibers heterostructures. The XRD pattern of bare TiO_2 nanofibers as the black curve shown in Fig. 4 reveals that the crystal phase of bare TiO_2 nanofibers was anatase with diffraction peaks at about $2\theta = 25.34^\circ$, 37.83°, 48.09°, 54.19°, and 55.03°, which could be perfectly indexed to the (1 0 1), (0 0 4), (2 0 0), (1 0 5), and (2 1 1) crystal faces of anatase TiO_2 (PDF file 21-1272, JCPDS) [25]. After being hydrothermally treated in the mixed solution of $Sr(NO_3)_2$ and NH_4OH at 180° for 48 h, additional diffraction peaks as the red curve shown in Fig. 4 with 2θ values of 32.55°, 39.91°, 46.43°, 57.94°, and 67.79° appeared, corresponding to (1 1 0), (1 1 1), (2 0 0), (2 1 1), and (2 2 0) crystal planes of cubic $SrTiO_3$, respectively (PDF file 34-734, JCPDS), indicating that part of TiO_2 was successfully converted into $SrTiO_3$ [22]. This

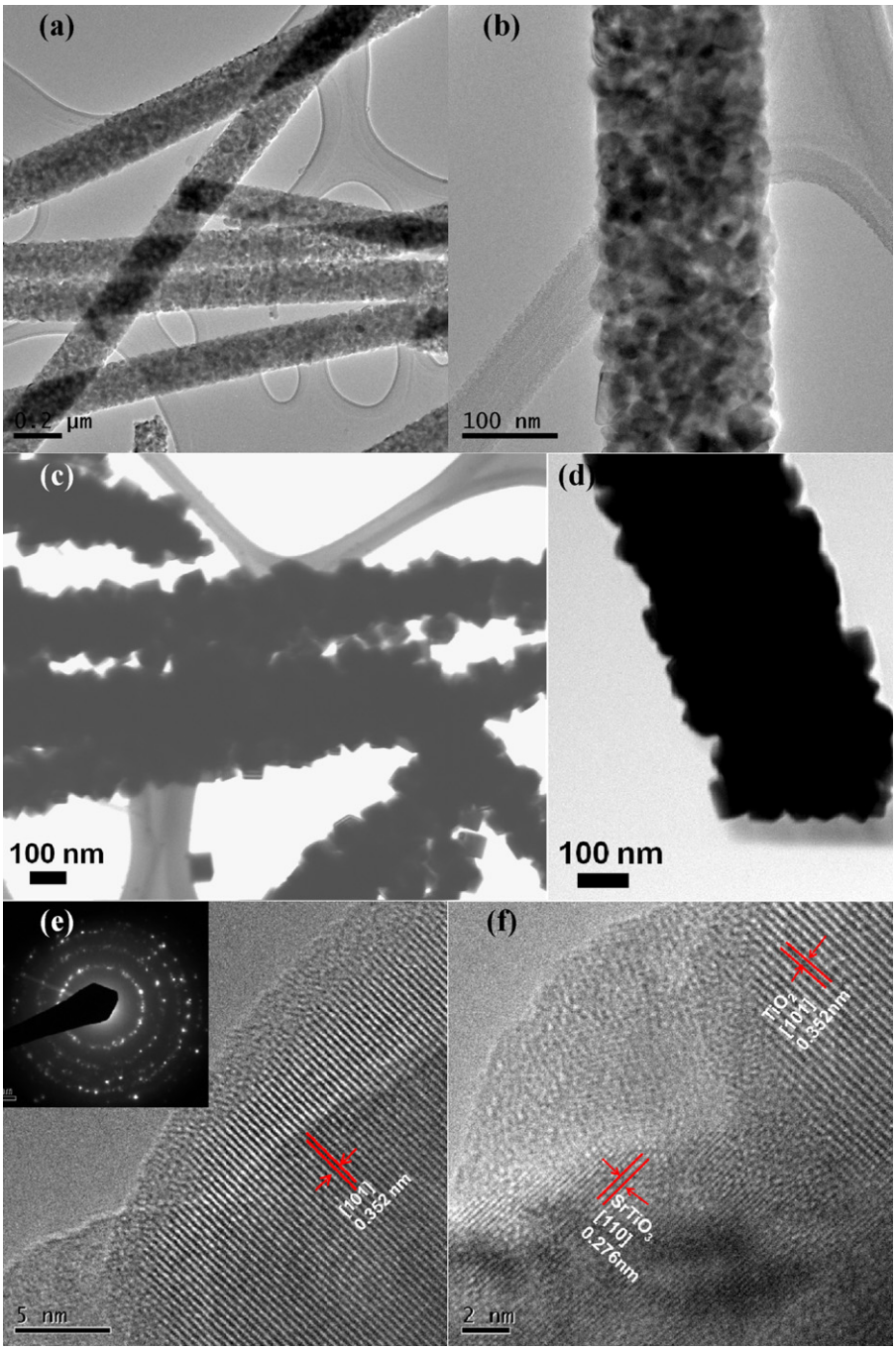

Fig. 3. (a) and (b) TEM image of bare TiO_2 nanofibers, (c) and (d) FESEM-STEM images of $SrTiO_3/TiO_2$ nanofibers heterostructures at different magnifications, (e) HRTEM image of bare TiO_2 nanofiber, inset is its corresponded selected area electron diffraction (SAED) pattern, and (f) HRTEM image of $SrTiO_3/TiO_2$ nanofibers heterostructures showing the overlapping zone of TiO_2 and $SrTiO_3$ in the heterostructures.

solidly confirmed that the $SrTiO_3/TiO_2$ nanofibers heterostructures have formed through continuously conducted electrospinning and hydrothermal process.

X-ray photoelectron spectroscopy (XPS) analysis was employed to further investigate the surface chemical composition and electronic structure of the $SrTiO_3/TiO_2$ nanofibers heterostructures. The binding energies and fwhm of the $SrTiO_3/TiO_2$ nanofibers heterostructures were listed out in Table 1. The XPS survey spectra as presented in Fig. 5a confirms the existence of Sr, Ti, and O in the $SrTiO_3/TiO_2$ nanofibers heterostructures. No other impurity elements, except carbon are present. The small carbon peak is inevitable in the XPS measurement [38]. The characteristic peaks of Ti 2p3/2 (457.564 eV) and Ti 2p1/2 (463.372 eV) in the high resolution spectrum of Ti 2p (Fig. 5b) match well with that of anatase TiO_2 [26]. The high resolution spectra of Sr 3d in Fig. 5c can be deconvoluted into two peaks for Sr 3d5/2 and Sr 3d3/2 located at 132.383 eV and 134.089 eV, respectively. The former peak at 132.383 eV is same as those reported for $SrTiO_3$ perovskite material and the latter peak at 134.089 eV can be ascribed to SrO complexes [39,40]. Two observable peaks from the high resolution O 1s spectra in Fig. 5d centered at 528.639 eV and 531.636 eV. The first peak is inherent to O atoms bound to metals such as Ti and Sr, while the latter peak is possibly ascribed to surface contamination by hydroxyl species [26].

Table 1
Binding energies (eV) and fwhm of the $SrTiO_3/TiO_2$ nanofibers heterostructures.

	Position (fwhm)	Position (fwhm)		Position (fwhm)	
	O 1s	Ti 2p3/2	Ti 2p1/2	Sr 3d5/2	Sr 3d3/2
$SrTiO_3/TiO_2$ nanofibers heterostructure	531.636 (2.764)528.639 (1.413)	457.564 (1.281)	463.372 (1.667)	132.383 (1.166)	134.089 (1.635)

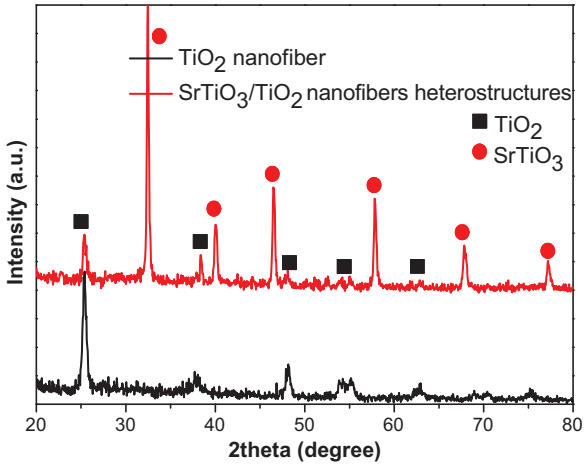

Fig. 4. XRD pattern of the $SrTiO_3/TiO_2$ nanofibers heterostructures and bare TiO_2 nanofibers. (For interpretation of the references to color in this figure legend, the reader is referred to the web version of the article.)

The porous structure of the bare TiO_2 nanofibers and $SrTiO_3/TiO_2$ nanofibers heterostructrues were revealed by N_2 adsorption/desorption isotherm curves in Fig. 6a. From Fig. 6a it is clear to see the typical mesoporous nature of the bare TiO_2 nanofibers and $SrTiO_3/TiO_2$ nanofibers heterostructures, which is in good agreement with the previous morphology observed by FESEM and TEM. From their corresponding pore size distribution curves in Fig. 6b, a dominant peak around 11 nm was observed for the bare TiO_2 nanofibers ascribing to the distance between different TiO_2 nanocrystals, while a smaller peak of 8 nm for $SrTiO_3/TiO_2$ nanofibers heterostructures arising from the distance between different $SrTiO_3$ cubics. The reduced pore size between $SrTiO_3$ in the $SrTiO_3/TiO_2$ nanofibers heterostructures in a comparison to bare TiO_2 nanofibers implies that $SrTiO_3$ was uniformly growth on the surface of TiO_2 nanofibers and close contact to each other, thus partially occupying the original pores on the surface of TiO_2 nanofibers and creating some smaller new pores. This is an obvious advantage over similar report, which $SrTiO_3$ cubic did not closely contact to each other [22]. It is interesting to note that the volume of $SrTiO_3/TiO_2$ nanofibers heterostructures at the given pore size of 8 nm was smaller than that of bare TiO_2 nanofibers at 11 nm, this reflects an even rougher surface was created by $SrTiO_3/TiO_2$ nanofibers heterostructures.

Besides, the BET specific surface of $SrTiO_3/TiO_2$ nanofibers heterostructures is measured to be 98.26 m^2/g, which is greater than that (50.08 m^2/g) of bare TiO_2 nanofibers. The enlarged specific surface area would create more reaction sites to facilitate the access of reactants. Considering the abovementioned advantages, it is reasonable to believe the hierarchical $SrTiO_3/TiO_2$ nanofibers heterostructures would be favorable for the improvement of photocatalytic activity [41,42].

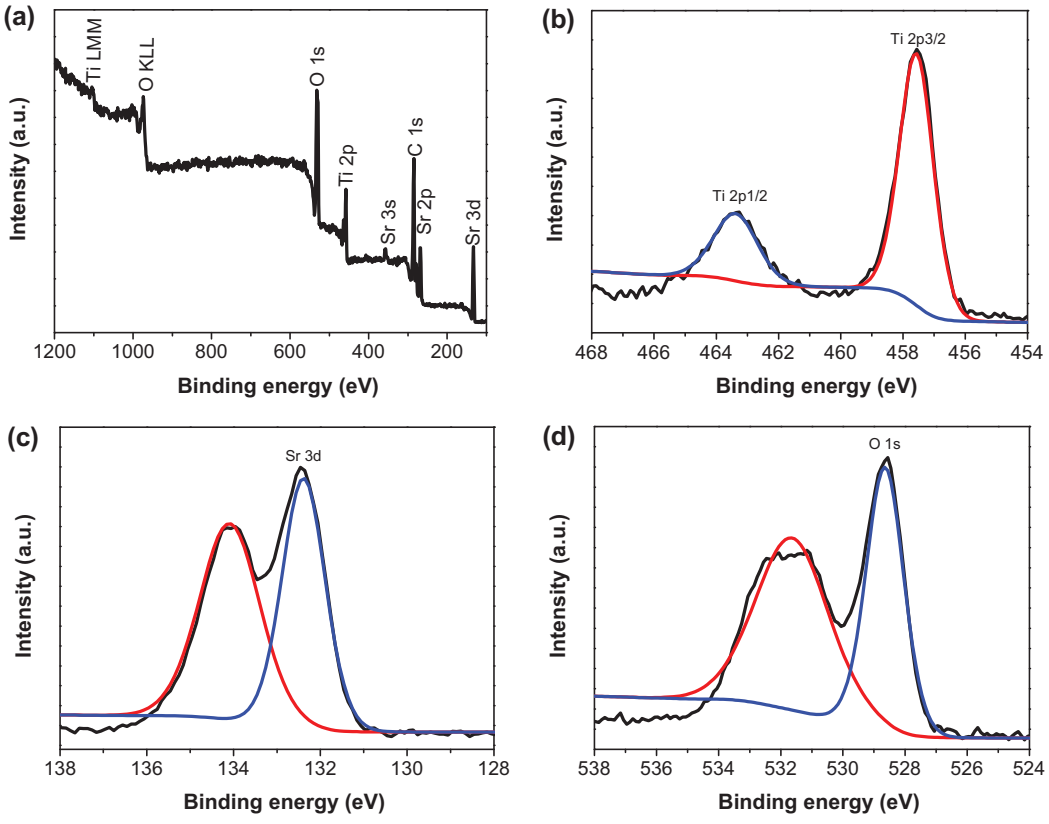

Fig. 5. (a) XPS survey spectra, and high resolution spectrum of (b) Ti 2p, (c) Sr 3d and (d) O 1s of the $SrTiO_3/TiO_2$ nanofibers heterostructures.

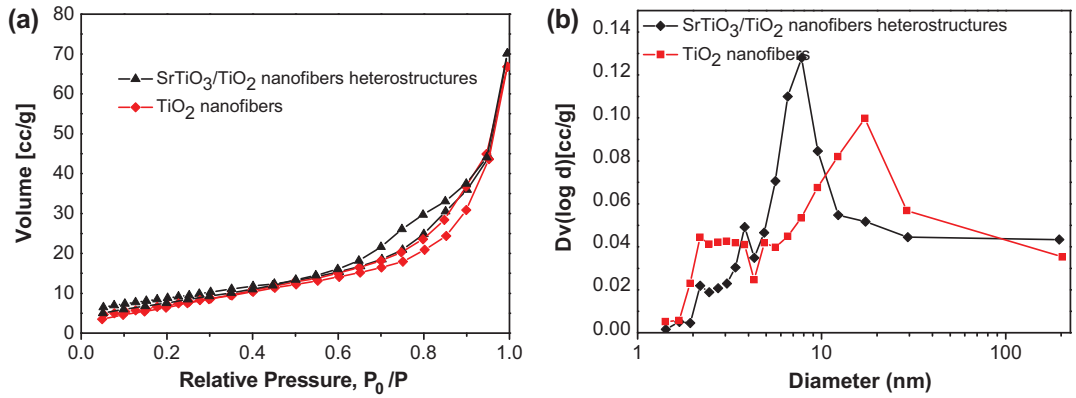

Fig. 6. (a) N_2 adsorption/desorption isotherm curves, and (b) BJH pore size distribution curves of the $SrTiO_3/TiO_2$ nanofibers heterostructures and bare TiO_2 nanofibers.

The light absorption capability of $SrTiO_3/TiO_2$ nanofibers heterostructures was investigated by a UV–vis spectrometer in a comparison to bare TiO_2 nanofibers as shown in Fig. 7. As our expected, the $SrTiO_3/TiO_2$ nanofibers heterostructures blue-shifts the absorption spectrum compared to bare TiO_2 nanofibers, after $SrTiO_3$ cubics with larger bandgap hydrothermally growing on the surface of bare TiO_2 nanofibers [26].

The Kubellka-Munk function was applied to convert diffusive reflectance measurements into the equivalent absorption coefficients [30].

$$\alpha = \frac{(1-R)^2}{2R} \quad (1)$$

where, α is optical absorption coefficient near the absorption edge for indirect interband transitions, R is the reflectance of the semiconductor, $R = 10^{-A}$, and A is an optical absorbance.

$$\alpha h\nu = C_1(h\nu - E_g)^2 \quad (2)$$

$$h\nu = \frac{1240}{\lambda} \quad (3)$$

where C_1 is the absorption constant for an indirect transition, $h\nu$ is the photo energy, E_g is the indirect bandgap energy (eV), and λ is the wavelength (nm).

The inset of Fig. 7 shows $(\alpha h\nu)^{1/2}$ plotted versus $h\nu$ and the vertical segment of the spectra is extended to intersect $h\nu$ axis (x-axis) to obtain the indirect bandgap (E_g) value of the $SrTiO_3/TiO_2$ nanofibers heterostructures and bare TiO_2 nanofibers. The $SrTiO_3/TiO_2$ nanofibers heterostructures slightly increased the bandgap compared to bare TiO_2 nanofibers. Evidently, the formation of $SrTiO_3/TiO_2$ heterojunctions modified the electronic structures of the bare TiO_2 nanofibers so as to leverage the separation of photogenerated electrons and holes thus benefiting the photocatalytic activity improvement.

3.2. Evaluation of photocatalytic H_2 generation

The H_2 generation activities of $SrTiO_3/TiO_2$ nanofibers heterostructures, bare $SrTiO_3$ nanocubics, and bare TiO_2 nanofibers were evaluated under the irradiation of UV light in a water/methanol sacrificial reagent system. Fig. 8 displays the H_2 evolution curves of $SrTiO_3/TiO_2$ nanofibers heterostructures, bare $SrTiO_3$ nanocubics, and bare TiO_2 nanofibers under the same conditions. Bare $SrTiO_3$ generated negligible H_2 owing to its low photocatalytic activity. Obviously, the $SrTiO_3/TiO_2$ nanofibers heterostructures exhibits better photocatalytic H_2 generation activity than bare TiO_2 nanofibers. During the same reaction period, $SrTiO_3/TiO_2$ nanofibers heterostructrues generated five times more H_2 than bare TiO_2 nanofibers. What is more, the photocatalytic H_2 generation rate of the $SrTiO_3/TiO_2$ nanofibers heterostructures is greater than that of bare TiO_2 nanofibers, indicating its high photocatalytic activity. A schematic diagram was drawn in Fig. 9 to elucidate the mechanism of the fast transfer of photogenerated electrons and holes in the $SrTiO_3/TiO_2$ nanofibers heterostructures [26]. Under the irradiation of UV light, electrons (e^-) in the CB of $SrTiO_3$ were excited and fast transferred to that of TiO_2 in the $SrTiO_3/TiO_2$ nanofibers heterostructures. The long

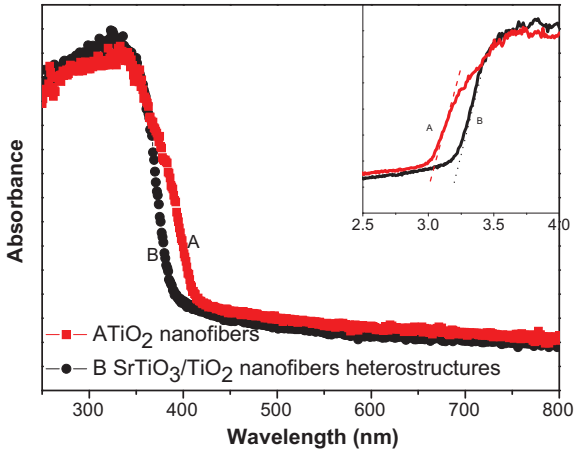

Fig. 7. UV–vis spectrum of the $SrTiO_3/TiO_2$ nanofibers heterostructures and bare TiO_2 nanofibers.

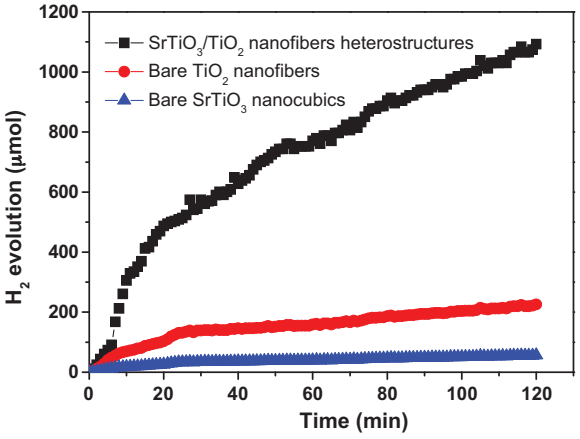

Fig. 8. H_2 evolution of the $SrTiO_3/TiO_2$ nanofibers heterostrutures and bare TiO_2 nanofibers under the irradiation of UV light in a water/methanol sacrificial reagent system.

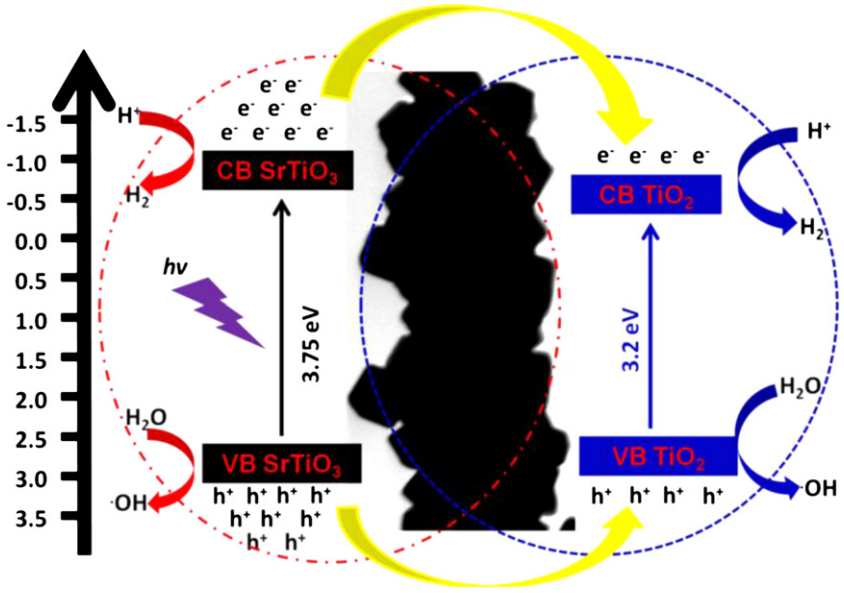

Fig. 9. Schematic diagram to elucidate the separation mechanism of photogenerated electrons and holes in the $SrTiO_3/TiO_2$ nanofibers heterostructures (indicated by the FESEM-STEM image at the middle of the diagram), methanol acting as sacrificial reagent scavenge the holes.

fibrous structure, hierarchical structure all play positive role in the separation process of photogenerated electrons and holes. The electrons were scavenged by protons (h^+) forming into H_2. While, the remaining holes in the VB of TiO_2 were transferred to that of $SrTiO_3$. In this water/methanol sacrificial reagent system, methanol acts as the scavengers to scavenge the holes and was finally mineralized [43,44]. In such a way, the recombination of photogenerated electrons and holes were suppressed effectively, and the photocatalytic activity is greatly enhanced. Furthermore, the hierarchical structure, the long fibrous structure, and the larger specific surface area of $SrTiO_3/TiO_2$ nanofibers heterostructures also benefit the photocatalytic activity synergistically.

4. Conclusion

Here, $SrTiO_3/TiO_2$ nanofibers heterostructrues have been successfully synthesized via continuously conducted electrospinning and hydrothermal method. The hydrothermal process greatly promotes the uniformly growing of $SrTiO_3$ cubics on the electrospun long TiO_2 nanofibers. The $SrTiO_3/TiO_2$ nanofibers heterostructrues synthesized in such a method possesses a lot of virtues such as fast separation of photogenerated electrons and holes owing to the synergistic effect of close contact between $SrTiO_3$ and TiO_2, 1D long fibrous structure, hierarchical structure property, and the larger specific surface area. All those virtues lead to high photocatalytic activity, which is proved by its higher photocatalytic H_2 generation activity than bare TiO_2 nanofibers under the same conditions.

References

[1] P.J. Hall, Energy Policy 36 (2008) 4363–4367.
[2] J. Alic, D. Sarewitz, C. Weiss, W. Bonvillian, Nature 466 (2010) 316–317.
[3] M.I. Hoffert, Science 329 (2010) 1292–1294.
[4] Z. Liu, H. Bai, J. Lee, D.D. Sun, Energy and Environmental Science 4 (2011) 2582–2585.
[5] M. Ashokkumar, International Journal of Hydrogen Energy 23 (1998) 427–438.
[6] A. Fujishima, K. Honda, Nature 238 (1972) 37–38.
[7] A. Kudo, Y. Miseki, Chemical Society Reviews 38 (2009) 253–278.
[8] X. Chen, S. Shen, L. Guo, S.S. Mao, Chemical Reviews 110 (2010) 6503–6570.
[9] J.H. Pan, H. Dou, Z. Xiong, C. Xu, J. Ma, X.S. Zhao, Journal of Materials Chemistry 20 (2010) 4512–4528.
[10] M.R. Hoffmann, S.T. Martin, W. Choi, D.W. Bahnemann, Chemical Reviews 95 (1995) 69–96.
[11] X. Chen, L. Liu, P.Y. Yu, S.S. Mao, Science 331 (2011) 746–750.
[12] N.J. Borys, M.J. Walter, J. Huang, D.V. Talapin, J.M. Lupton, Science 330 (2010) 1371–1374.
[13] A. Fujishima, X. Zhang, D.A. Tryk, Surface science reports 63 (2008) 515–582.
[14] J. Ng, J.H. Pan, D.D. Sun, Journal of Materials Chemistry 21 (2011) 11844–11853.
[15] X. Zhang, T. Zhang, J. Ng, D.D. Sun, Advanced Functional Materials 19 (2009) 3731–3736.
[16] T. Krishnamoorthy, V. Thavasi, M. Subodh, G.S. Ramakrishna, Energy & Environmental Science 4 (2011) 2807–2812.
[17] Y. Lin, G. Yuan, R. Liu, S. Zhou, S.W. Sheehan, D. Wang, Chemical Physics Letters 507 (2011) 209–215.
[18] G.K. Mor, O.K. Varghese, R.H.T. Wilke, S. Sharma, Nano Letters 8 (2008) 1906–1911.
[19] A. Greiner, J.H. Wendorff, Angewandte Chemie International Edition 46 (2007) 5670–5703.
[20] J.T. McCann, D. Li, Y. Xia, Journal of Materials Chemistry 15 (2005) 735–738.
[21] D. Li, Y. Wang, Y. Xia, Nano Letters 3 (2003) 1167–1171.
[22] T. Cao, Y. Li, C. Wang, C. Shao, Y. Liu, Langmuir 27 (2011) 2946–2952.
[23] Z. Liu, D.D. Sun, P. Guo, J.O. Leckie, Nano Letters 7 (2007) 1081–1085.
[24] R. Ostermann, D. Li, Y. Yin, J.T. McCann, Y. Xia, Nano Letters 6 (2006) 1297–1302.
[25] H. Bai, Z. Liu, D.D. Sun, Applied Catalysis B: Environmental 111–112 (2012) 571–577.
[26] J. Ng, S. Xu, X. Zhang, H.Y. Yang, D.D. Sun, Advanced Functional Materials 20 (2010) 4287–4294.
[27] R.G. Carr, G.A. Somorjai, Nature 290 (1981) 576–577.
[28] K. Sayama, K. Mukasa, R. Abe, Y. Abe, H. Arakawa, Journal of Photochemistry and Photobiology A: Chemistry 148 (2002) 71–77.
[29] S. Ardo, G.J. Meyer, Chemical Society Reviews 38 (2009) 115–165.
[30] H. Bai, Z. Liu, D.D. Sun, Physical Chemistry Chemical Physics 13 (2011) 6205–6210.
[31] M.G. Mckee, J.M. Layman, M.P. Cashion, T.E. Long, Science 311 (2006) 353–355.
[32] D. Li, Y. Xia, Nano Letters 3 (2003) 555–560.
[33] J. Zhang, J.H. Bang, C. Tang, P.V. Kamat, ACS Nano 4 (2010) 387–395.
[34] S. Xu, A.J. Du, J. Liu, J. Ng, D.D. Sun, International Journal of Hydrogen Energy 36 (2011) 6538–6545.
[35] S. Xu, D.D. Sun, International Journal of Hydrogen Energy 34 (2009) 6096–6104.
[36] F.D. Fonzo, C.S. Casari, V. Russo, M.F. Brunella, A.L. Bassi, C.E. Bottani, Nanotechnology 20 (2009) 015604.
[37] Y. Zhao, X. Zhang, J. Zhai, J. He, L. Jiang, Z. Liu, S. Nishimoto, T. Murakami, A. Fujishima, D. Zhu, Applied Catalysis B: Environmental 83 (2008) 24–29.
[38] Z. Liu, H. Bai, S. Xu, D.D. Sun, International Journal of Hydrogen Energy 36 (2011) 13473–13480.
[39] W.D. Yang, Journal of Materials Science 34 (1999) 3533–3544.
[40] R.P. Vasquez, Journal of Electron Spectroscopy and Related Phenomena 56 (1991) 217–240.
[41] H. Bai, Z. Liu, D.D. Sun, Chemical Communications 46 (2010) 6542–6544.
[42] J.H. Pan, X. Zhang, A.J. Du, D.D. Sun, J.O. Leckie, Journal of American Chemical Society 130 (2008) 11256–11257.
[43] S. Xu, J. Ng, X. Zhang, H. Bai, D.D. Sun, International Journal of Hydrogen Energy 35 (2010) 5254–5261.
[44] S. Xu, J. Ng, A.J. Du, J. Liu, D.D. Sun, International Journal of Hydrogen Energy 36 (2011) 6538–6545.